Neoadjuvant chemotherapy enhances anti-tumor immune response of tumor microenvironment in human esophageal squamous cell carcinoma

奥田, 翔

iScience

CellPress
OPEN ACCESS

Article

Neoadjuvant chemotherapy enhances anti-tumor immune response of tumor microenvironment in human esophageal squamous cell carcinoma

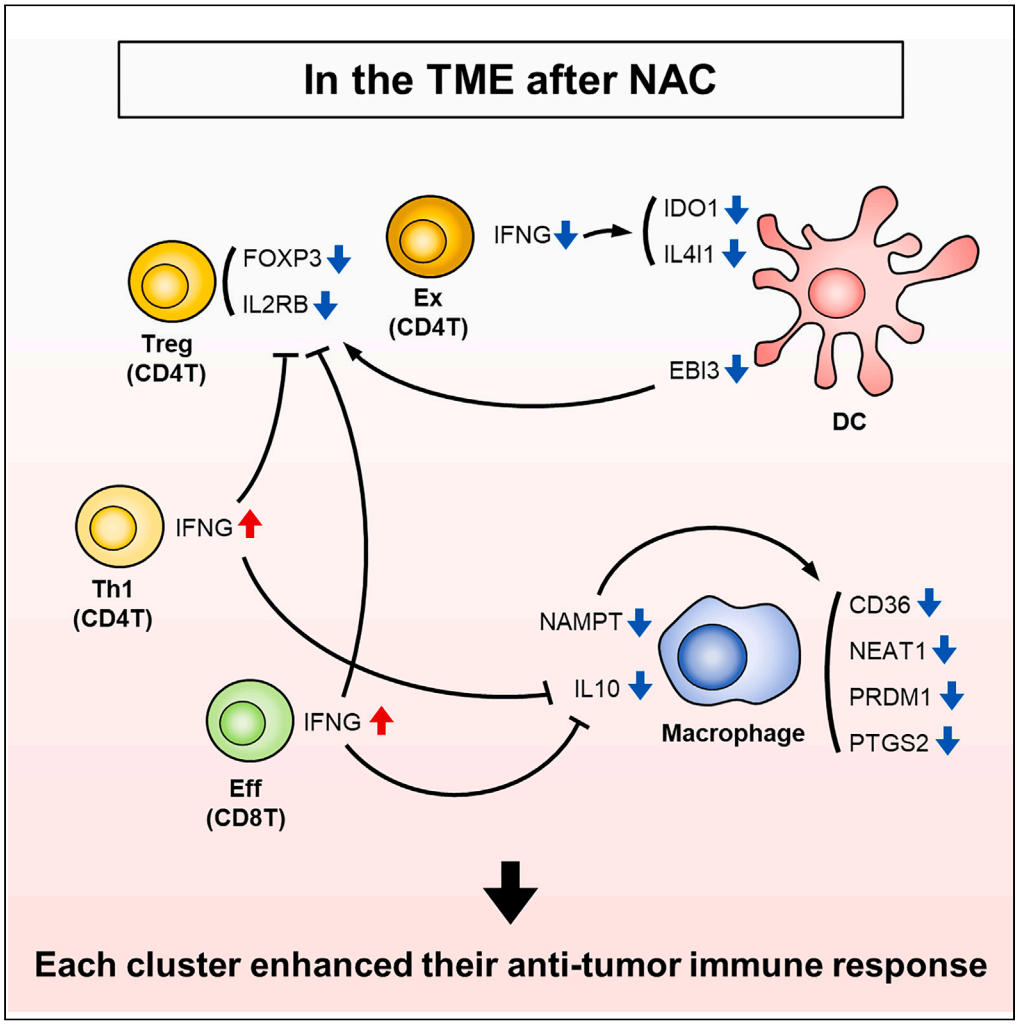

Sho Okuda, Kenoki Ohuchida, Shoichi Nakamura, ..., Takanari Kitazono, Yoshinao Oda, Masafumi Nakamura

ouchida.kenoki.060@m.kyushu-u.ac.jp

Highlights

We investigated the impact of NAC on immune cells in human ESCC using scRNA-seq

The immune cell clusters in ESCC enhanced their anti-tumor functions after NAC

Such clusters interacted with each other via multiple molecules

NAC enhances the anti-tumor immune response via various clusters in the TME of ESCC

Okuda et al., iScience 26, 106480
April 21, 2023
https://doi.org/10.1016/j.isci.2023.106480

iScience

CellPress
OPEN ACCESS

Article

Neoadjuvant chemotherapy enhances anti-tumor immune response of tumor microenvironment in human esophageal squamous cell carcinoma

Sho Okuda,[1] Kenoki Ohuchida,[1,5,*] Shoichi Nakamura,[1] Chikanori Tsutsumi,[1] Kyoko Hisano,[1] Yuki Mochida,[1] Jun Kawata,[2] Yoshiki Ohtsubo,[1] Tomohiko Shinkawa,[1] Chika Iwamoto,[1] Nobuhiro Torata,[1] Yusuke Mizuuchi,[1] Koji Shindo,[1] Taiki Moriyama,[1] Kohei Nakata,[1] Takehiro Torisu,[3] Takashi Morisaki,[4] Takanari Kitazono,[3] Yoshinao Oda,[2] and Masafumi Nakamura[1]

SUMMARY

Although chemotherapy has been an essential treatment for cancer, the development of immune checkpoint blockade therapy was revolutionary, and a comprehensive understanding of the immunological tumor microenvironment (TME) has become crucial. Here, we investigated the impact of neoadjuvant chemotherapy (NAC) on immune cells in the TME of human esophageal squamous cell carcinoma using single cell RNA-sequencing. Analysis of 30 fresh samples revealed that CD8+/CD4+ T cells, dendritic cells (DCs), and macrophages in the TME of human esophageal squamous cell carcinoma showed higher levels of an anti-tumor immune response in the NAC(+) group than in the NAC(−) group. Furthermore, the immune cells of the NAC(+) group interacted with each other resulting in enhanced anti-tumor immune response via various cytokines, including *IFNG* in CD8+/CD4+ T cells, *EBI3* in DCs, and *NAMPT* in macrophages. Our results suggest that NAC potentially enhances the anti-tumor immune response of immune cells in the TME.

INTRODUCTION

Esophageal cancer is the seventh most common cancer worldwide.[1] In Japan, more than 85% of esophageal cancers are esophageal squamous cell carcinoma (ESCC).[2] Neoadjuvant therapy including chemotherapy and/or radiotherapy is recommended for advanced esophageal cancer to improve patient prognosis by downstaging of the tumor[3] and controlling local and distant micrometastasis.[4] Despite the advances in neoadjuvant therapy improved surgical techniques and better patient selection, the 5-year recurrence-free survival (RFS) rate after neoadjuvant therapy followed by esophagectomy is only approximately 50%.[5] Therefore, novel treatments are required to improve patient prognosis.

In recent years, the study of the tumor microenvironment (TME) from an immunological perspective, and the advent of immune checkpoint blockade (ICB) for cancer treatment have been focuses of intensive research. Expression of PD-L1, one of the ICBs, in ESCC bulk tissue was associated with poor prognosis,[6] and ICB was shown to significantly prolong overall survival over chemotherapy in unresectable or recurrent ESCC.[7] However, the median overall survival rate with ICB is only 10.9 months and remains unsatisfactory. Previous reports showed that PD-L1 expression was increased in TME-infiltrating $CD8^+$ T cells (CD8T) after neoadjuvant chemotherapy (NAC) of ESCC[8] and cervical cancer.[9] These results suggest that NAC alters the immunological TME. Therefore, better understanding of the effects of NAC on the immune status in the TME of ESCC will be extremely valuable in guiding the selection of appropriate treatment combinations including ICB.

Single cell RNA-sequencing (scRNA-seq), a method to comprehensively analyze the global mRNA expression in a single cell, has become widely used worldwide and is useful for analyzing the transitional status of various types of immune cells in the TME with complicated heterogeneity. In recent years, scRNA-seq has been applied to various human cancers, such as melanoma,[10] lung cancer,[11] colorectal cancer,[12] breast cancer,[13] and ESCC.[14] These studies have revealed the heterogeneity of the TME with novel immune

[1]Department of Surgery and Oncology, Graduate School of Medical Sciences, Kyushu University, Fukuoka 812-8582, Japan

[2]Department of Anatomic Pathology, Pathological Sciences, Graduate School of Medical Sciences, Kyushu Hospital, Fukuoka 812-8582, Japan

[3]Department of Medicine and Clinical Science, Graduate School of Medical Sciences, Kyushu University, Fukuoka 812-8582, Japan

[4]Department of Cancer Immunotherapy, Fukuoka General Cancer Clinic, Fukuoka 812-0018, Japan

[5]Lead contact

*Correspondence: ouchida.kenoki.060@m.kyushu-u.ac.jp

https://doi.org/10.1016/j.isci.2023.106480

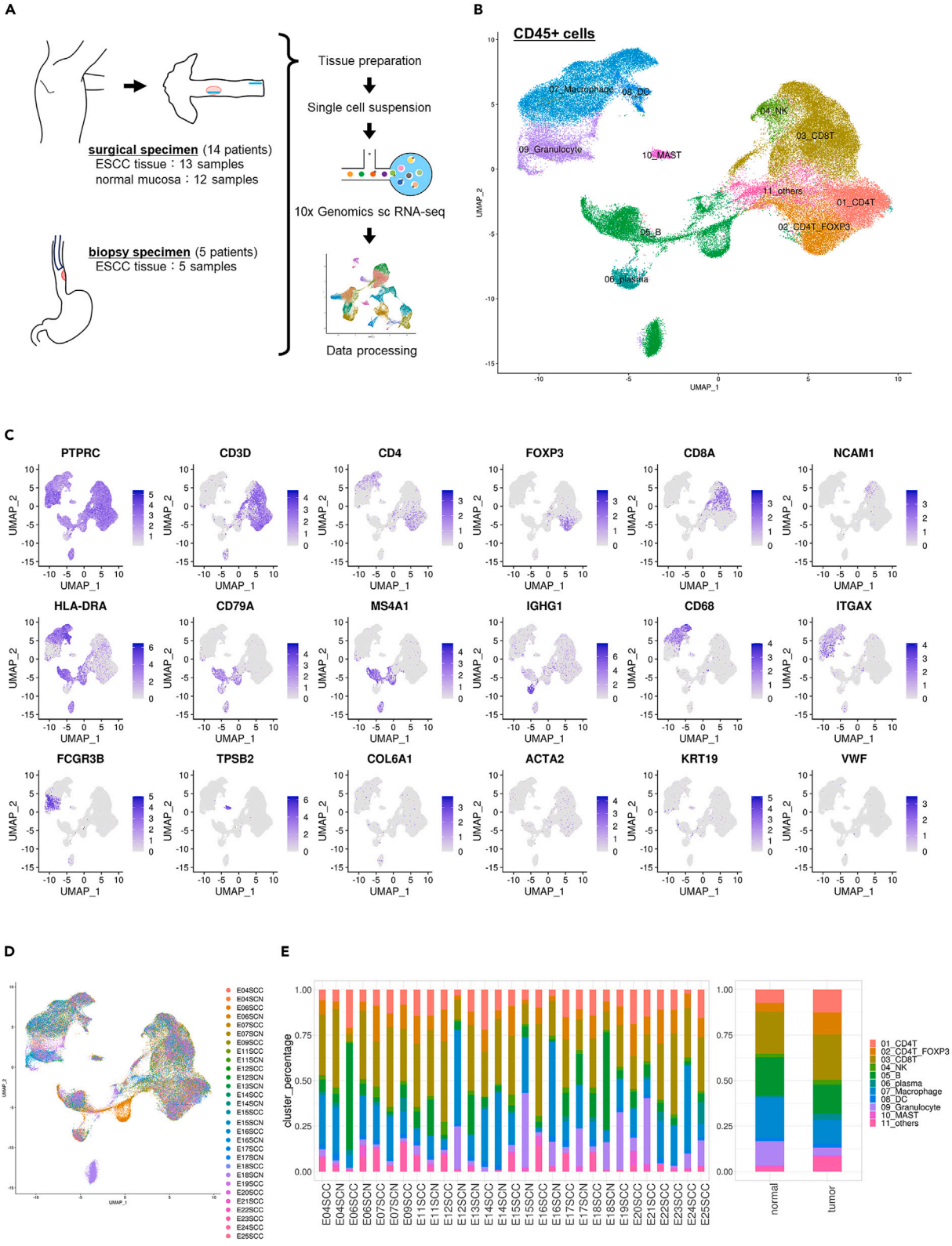
A
surgical specimen (14 patients)
ESCC tissue : 13 samples
normal mucosa : 12 samples
biopsy specimen (5 patients)
ESCC tissue : 5 samples
Tissue preparation
Single cell suspension
10x Genomics sc RNA-seq
Data processing
B
CD45+ cells
07_Macrophage
08_DC
04_NK
03_CD8T
09_Granulocyte
10_MAST
11_others
01_CD4T
02_CD4T_FOXP3
05_B
06_plasma
UMAP_1
UMAP_2
C
PTPRC
CD3D
CD4
FOXP3
CD8A
NCAM1
HLA-DRA
CD79A
MS4A1
IGHG1
CD68
ITGAX
FCGR3B
TPSB2
COL6A1
ACTA2
KRT19
VWF
D
E
cluster_percentage
normal
tumor
01_CD4T
02_CD4T_FOXP3
03_CD8T
04_NK
05_B
06_plasma
07_Macrophage
08_DC
09_Granulocyte
10_MAST
11_others

Figure 1. scRNA-seq classifies CD45$^+$ cells into clusters of known cell types

(A) Experimental design and analysis.

(B) UMAP plot of 83,151 CD45$^+$ cells after quality check, normalization, and exclusion of doublets and contamination cells. The cell type was determined based on the expression of known marker genes.

(C) Expression of representative marker genes in UMAP.

(D) The location of the cells in each sample in the UMAP.

(E) Percentage of cell types by (left) sample, and (right) normal mucosa, and tumor tissue. **ESCC**, esophageal squamous cell carcinoma; **CD4T**, CD4$^+$ T cells; **CD4T_FOXP3**, CD4$^+$ FOXP3+ T cells; **CD8T**, CD8$^+$ T cells; **NK**, natural killer cells; **B**, B cells; **plasma**, plasma cells; **DC**, dendritic cells; **SCC**, tumor tissue; **SCN**, normal mucosa.

See also Figure S1 and Table S1.

cell subsets including diverse immunosuppressive populations. However, there have been no reports examining the changes in the TME associated with therapeutic interventions in human ESCC using scRNA-seq.

In this study, we performed scRNA-seq on 18 human ESCC tissues and 12 human normal esophageal tissues with squamous cell mucosa collected from surgically resected specimens or biopsied specimens under gastroscopy to analyze the CD45$^+$ cell population. We focused on functional clusters of CD8T, CD4$^+$ T cells (CD4T), dendritic cells (DCs), and macrophages (Mφ), and examined NAC-induced changes in the immune status and function. Our results showed that NAC increased the anti-tumor functions in each immune cell type. We further analyzed the interactions among the functional clusters in each immune cell type to determine the mechanism underlying the enhanced anti-tumor immune function. Our results suggest that NAC induces immunological changes in the TME of ESCC, possibly resulting in the enhancement of anti-tumor function in various immune cell types.

RESULTS

scRNA-seq classifies CD45$^+$ cells into clusters of known cell types

We collected 18 ESCC tissues and 12 normal tissues with esophageal mucosa from 19 patients (Table S1) and performed scRNA-seq. CD45$^+$ cell data were extracted from all data and analyzed (Figure 1A). After removing low-quality cells, we obtained 178,333 cells (Figure S1A). After excluding cells suspected of doublet or contamination on the basis of gene expression levels and types (Figure S1B), 83,151 cells were finally included in this analysis (Figure 1B). A total of 10 clusters were identified, and the cell type of each cluster was determined from representative gene expression, as shown in Figure 1C. Batch effect removal and normalization in data processing were sufficiently performed (Figure 1D). The present study included both biopsy and surgical specimens; there were no substantial differences in the numerical balance for most of the clusters except for the proportion of B cells and granulocytes that were not handled in this analysis (Figure S1C). The proportions of each cluster in each sample are shown in Figure 1E. In the comparison of the normal mucosa and tumor tissue (Figure 1E), the percentages of CD8T and CD4T including *FOXP3*+ cells were higher in the tumor tissue samples than those in the normal mucosa samples, while the percentage of macrophages and neutrophils was lower. These results showed that the cells were divided into known cell types, and the proportions of cell types differed between normal mucosa and tumor tissue.

NAC enhances the anti-tumor immune response in each cluster of CD8T in the TME by reducing apoptosis, promoting memorization, and preventing exhaustion

From the cells of Figure 1B, we extracted CD3$^+$ CD8$^+$ cells as CD8T (Figure S2A) and obtained 11,264 cells. When the doublet and contamination cells were removed (Figure S2B), 8,005 cells remained (Figure 2A, Figure S2C). The remained CD8T cells were divided into six clusters in the re-analysis that were determined to be naive (N), central memory (CM), effector memory (EM), effector (Eff), proliferative exhaust (Ex_MKI67), and exhaust (Ex) clusters on the basis of expression levels of differential expressed genes (DEGs) (Figure 2B, Table S2) and representative genes (Figure 2C, Figure S2D). In the comparison of the percentage of cells assigned to each cluster between normal mucosa and tumor tissue, the results showed that tumor tissues consisted of more Ex_MKI67 and fewer Eff cells than normal tissues (Figure 2D). Although there was no remarkable difference in the percentage of Ex cells between normal mucosa and tumor tissue, the expressions of exhaust genes (*PDCD1*, *LAG3*, and *HAVCR2*) in the Ex cluster were significantly higher in the tumor tissue ($p < 0.0001$) (Figure 2E).

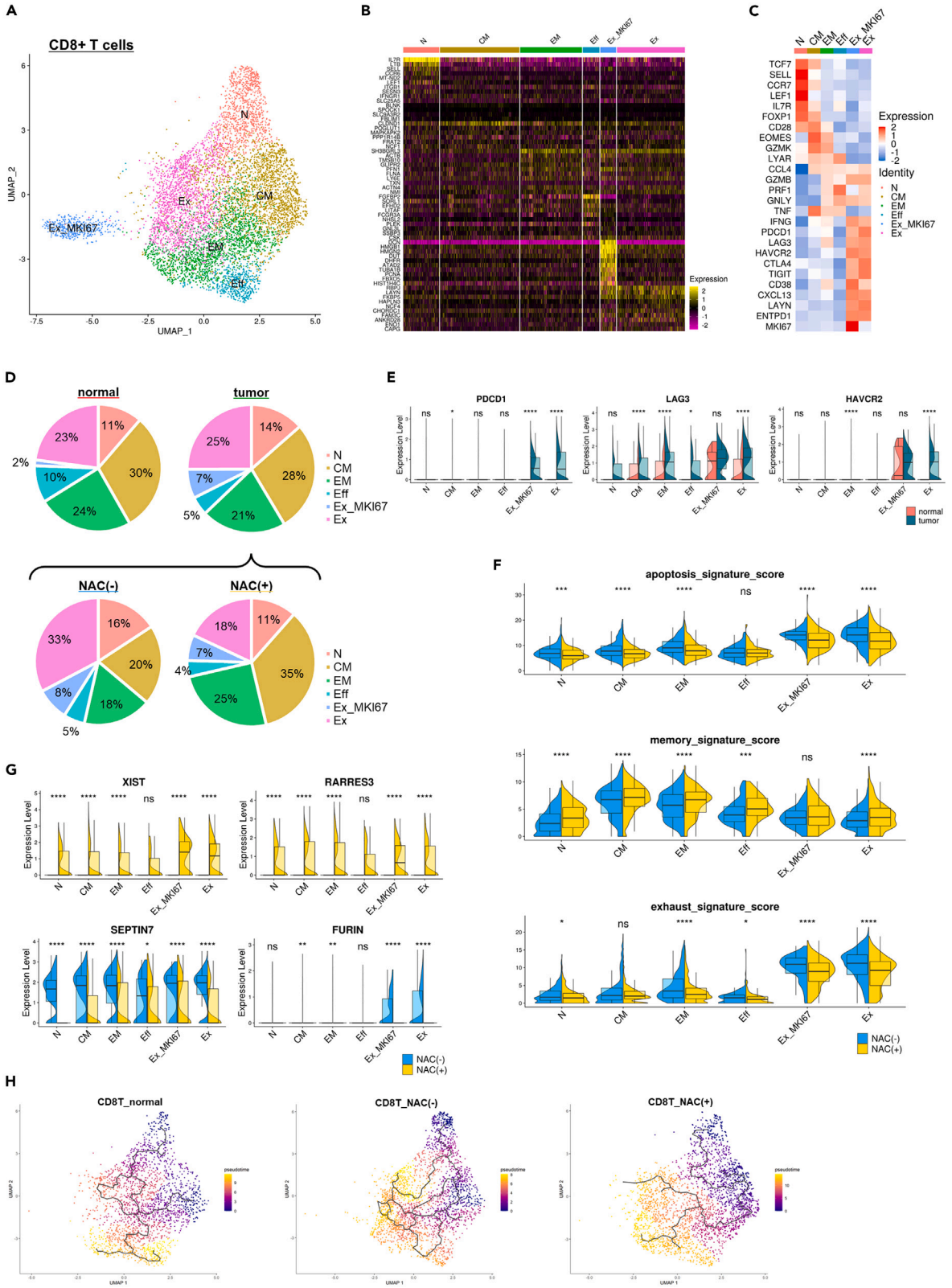
A
CD8+ T cells
UMAP_2
UMAP_1
N
CM
EM
Eff
Ex
Ex_MKI67
B
Expression
C
TCF7
SELL
CCR7
LEF1
IL7R
FOXP1
CD28
EOMES
GZMK
LYAR
CCL4
GZMB
PRF1
GNLY
TNF
IFNG
PDCD1
LAG3
HAVCR2
CTLA4
TIGIT
CD38
CXCL13
LAYN
ENTPD1
MKI67
Expression
Identity
D
normal
tumor
11%
23%
2%
10%
30%
24%
14%
25%
7%
28%
5%
21%
NAC(-)
NAC(+)
16%
33%
20%
8%
18%
5%
18%
11%
7%
4%
35%
25%
E
PDCD1
LAG3
HAVCR2
Expression Level
normal
tumor
F
apoptosis_signature_score
memory_signature_score
exhaust_signature_score
G
XIST
RARRES3
SEPTIN7
FURIN
Expression Level
NAC(-)
NAC(+)
H
CD8T_normal
CD8T_NAC(-)
CD8T_NAC(+)
pseudotime

Figure 2. NAC enhances the anti-tumor immune response in each cluster of CD8T in the TME by reducing apoptosis, promoting memorization, and preventing exhaustion

(A) UMAP plot of 8,005 $CD8^+$ T cells extracted from $CD45^+$ cells. The function of each cluster was determined based on the gene expression.

(B) Heatmap used as the basis for clustering. In each cluster, the top 10 genes with significantly higher expression than in other clusters are shown.

(C) Heatmap of representative gene expression in each cluster.

(D) Percentage of the number of cells composing each cluster. The top charts show normal mucosa and tumor tissue, and the bottom charts are shown by the presence of NAC in the tumor tissue.

(E) Comparison of exhaust gene expression in normal mucosa and tumor tissue. The violin plots were drawn based on the number of genes expressed in each cell.

(F) Comparison of signature gene expression in tumor tissue with and without NAC. The violin plots were drawn based on the scored signature gene expression in each cell.

(G) Comparison of *XIST*, *RARRES3*, *SEPTIN7*, and *FURIN* gene expression in tumor tissue with and without NAC. The violin plots were drawn on the basis of the number of genes expressed in each cell.

(H) Trajectory analysis of normal mucosa, tumor tissue without NAC, and tumor tissue with NAC. The pseudotime trajectory was calculated with darker colors indicating older and lighter colors indicating newer. **CD8T**, $CD8^+$ T cell; **N**, naive CD8T; **CM**, central memory CD8T; **EM**, effector memory CD8T; **Eff**, effector CD8T; **Ex_MKI67**, proliferative exhausted CD8T; **Ex**, exhausted CD8T; **normal**, normal mucosa; **tumor**, tumor tissue; **NAC**, neoadjuvant chemotherapy; **ns**, not significant; *, $p < 0.05$; **, $p < 0.01$; ***, $p < 0.001$; ****, $p < 0.0001$.

See also Figures S2, S3, Tables S2, and S3.

We compared the cells in the NAC(+) group with those in the NAC(−) group. There were more CM and EM cells and fewer Ex cells in the NAC(+) group than those in the NAC(−) group (Figure 2D). The expression levels of the memory, exhaust, and apoptosis signatures (Table S3) were scored and compared between the NAC(+) and NAC(−) groups (Figure 2F). The NAC(+) group showed a significantly higher memory signature score in all clusters except the Ex_MKI67 cluster than in the NAC(−) group. The NAC(+) group showed significantly lower exhaust signature scores in all clusters except the CM cluster and lower apoptosis signature scores in all clusters except the Eff cluster than in the NAC(−) group. To avoid the effect of the difference between biopsy and surgical samples, we performed the same analyses using the data only from surgical samples and found the similar significant differences in the signature scores between the NAC(+) and NAC(−) groups (Figure S3).

We analyzed the DEGs in each cluster between NAC(+) and NAC(−) groups. Among the DEGs, *XIST*, whose suppression renders ovarian cancer chemotherapy resistant,[15] and *RARRES3*, whose high expression suppresses breast cancer metastasis[16] were highly expressed on tumor-infiltrating CD8T in the NAC(+) group (Figure 2G). The expressions of *SEPTIN7* and *FURIN*, known risk factors for the carcinogenesis of various carcinomas[17,18] were significantly lower in the CD8T of the NAC(+) group (Figure 2G).

We also performed trajectory analysis for CD8T in normal mucosa and tumor tissue (Figure 2H). The Ex_MKI67 cluster was not analyzed because the cell cycle-related genes affect trajectories. NAC(−) group cells had various trajectories to the Ex cluster including the trajectory directly from the N cluster. However, in the NAC(+) group, the trajectory to the Ex cluster was limited to the path from EM and there was no direct trajectory from the N cluster to the Ex cluster.

These findings suggest that NAC reduced apoptosis, promoted memorization, and prevented exhaustion in each cluster of CD8T resulting in an enhanced anti-tumor immune response.

NAC promotes the anti-tumor immune response in each cluster of CD4T

To analyze CD4T, *CD3D* + *CD4*$^+$ cells were extracted from the $CD45^+$ cells (Figure S4A). The cell count was 7,977 cells, and 6,453 cells remained after doublet and contamination removal (Figures 3A, S4B, and S4C). CD4T were divided into six clusters, naive (N), follicular helper T (Tfh), type 1 helper T (Th1), Exhaust (Ex), proliferative regulatory T (Treg_MKI67), and regulatory T (Treg) cluster, on the basis of gene expression (Figures 3B and 3C, Figure S4D, and Table S2). We compared CD4T clusters between normal mucosa and tumor tissue and found that tumor tissue had fewer N and more Treg cells than that in normal tissue (Figure 3D). We also found clusters of Tfh cells, which are responsible for antigen presentation from B cells in lymph nodes in both normal mucosa and tumor tissue (Figure 3D). Cytotoxic genes (*GZMB*, *PRF1*, *GNLY*, and *KLRG1*) were expressed predominantly in the Th1 cluster and their expression was weaker in tumor tissue than that in normal mucosa (Figure 3E). Similar to the results observed in CD8T, the expression levels of exhaust genes (*PDCD1*, *LAG3*, *HAVCR2*, and *TIGIT*) were significantly higher in the CD4T Ex cluster of tumor tissue than in that of normal tissue (Figure 3E). Treg-related genes (*CTLA4*, *FOXP3*, and *IL2RA*) were also highly expressed in the Treg cluster and Treg_MKi67 cluster of tumor tissue compared with

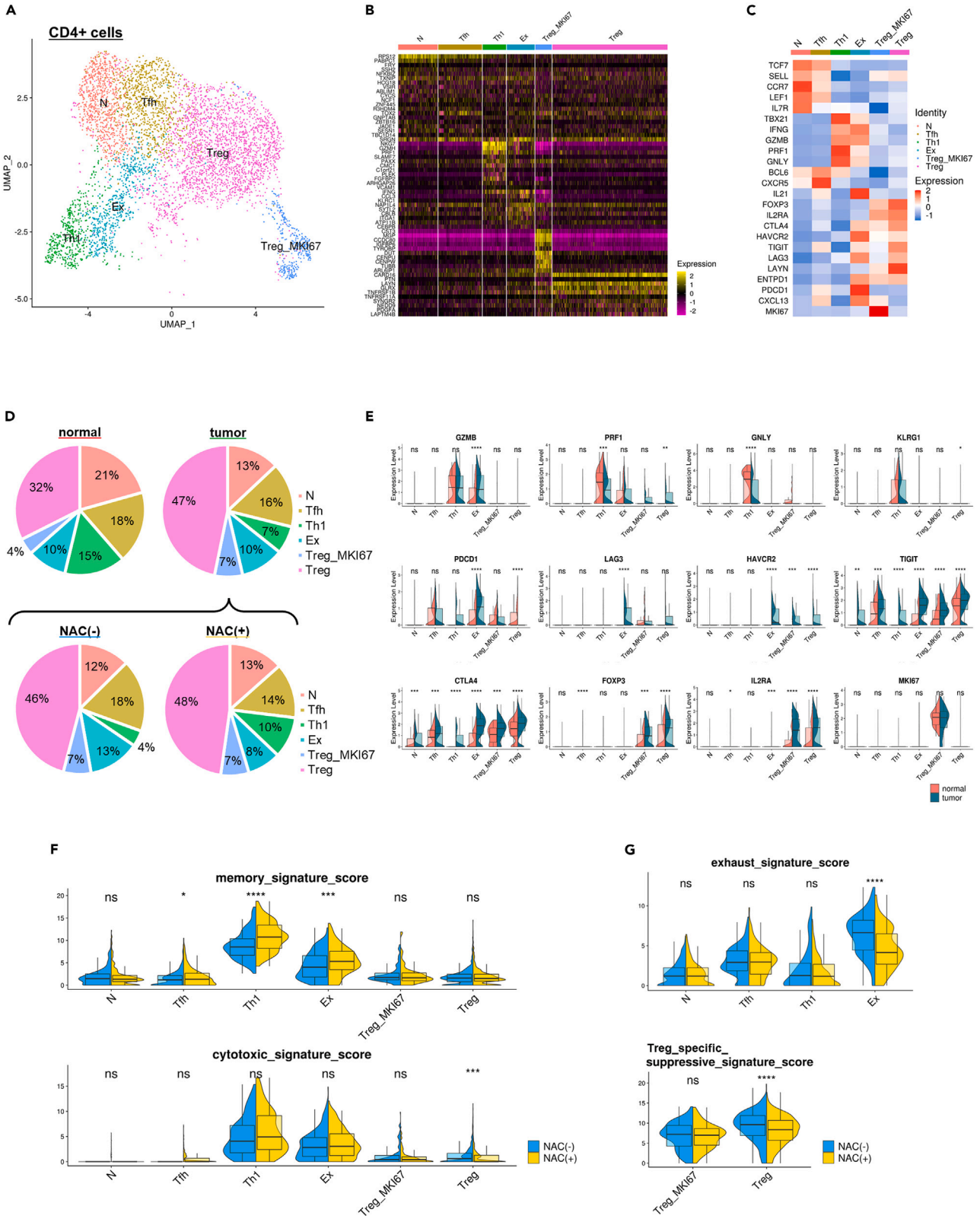
A
CD4+ cells
N
Tfh
Th1
Ex
Treg
Treg_MKI67
UMAP_1
UMAP_2
B
Expression
C
Identity
Expression
TCF7
SELL
CCR7
LEF1
IL7R
TBX21
IFNG
GZMB
PRF1
GNLY
BCL6
CXCR5
IL21
FOXP3
IL2RA
CTLA4
HAVCR2
TIGIT
LAG3
LAYN
ENTPD1
PDCD1
CXCL13
MKI67
D
normal
tumor
NAC(-)
NAC(+)
E
GZMB
PRF1
GNLY
KLRG1
PDCD1
LAG3
HAVCR2
TIGIT
CTLA4
FOXP3
IL2RA
MKI67
Expression Level
normal
tumor
F
memory_signature_score
cytotoxic_signature_score
NAC(-)
NAC(+)
G
exhaust_signature_score
Treg_specific_
suppressive_signature_score

Figure 3. NAC promotes the anti-tumor immune response in each cluster of CD4T

(A) UMAP plot of 6,453 $CD4^+$ T cells extracted from $CD45^+$ cells. The function of each cluster was determined based on the gene expression.

(B) Heatmap used as the basis for clustering. In each cluster, the top 10 genes with significantly higher expression than the expressions in the other clusters are shown.

(C) Heatmap of representative gene expression in each cluster.

(D) Percentage of the number of cells composing each cluster. The top graphs show normal mucosa and tumor tissue, and the bottom graphs are shown by the presence of NAC in the tumor tissue.

(E) Comparison of various gene expression in normal mucosa and tumor tissue. The violin plots were drawn based on the number of genes expressed in each cell.

(F and G) Comparison of signature gene expression in tumor tissue with and without NAC. The violin plots were drawn based on the scored signature gene expression in each cell. **CD4T**, $CD4^+$ T cell; **N**, naive CD4T; **Tfh**, follicular helper CD4T; **Th1**, type 1 helper CD4T; **Ex**, exhausted CD4T; **Treg_MKI67**, proliferative regulatory CD4T; **Treg**, regulatory CD4T; **normal**, normal mucosa; **tumor**, tumor tissue; **NAC**, neoadjuvant chemotherapy; **ns**, not significant; *, $p < 0.05$; **, $p < 0.01$; ***, $p < 0.001$; ****, $p < 0.0001$.

See also Figures S4, S5, Tables S2, and S3.

expressions in normal tissue (Figure 3E). All clusters of CD4T expressed *CTLA4* at a higher level in tumor tissues than those in normal tissues (Figure 3E).

The NAC(+) group had more Th1 cells in CD4T than the NAC(−) group (Figure 3D). We compared CD4T function-related gene expression levels of tumor tissue between NAC(+) and NAC(−) groups using memory and cytotoxic signatures (Table S2, Figure 3F). The NAC(+) group showed a significantly higher memory signature score in Tfh, Th1, and Ex clusters than the NAC(−) group. There was no difference in the cytotoxic signature scores between NAC(−) and NAC(+) groups, although there was a significant difference in the Treg cluster. In the comparison of exhaust signature scores in the N, Tfh, Th1, and Ex clusters (Table S2) between NAC(−) and (+) groups, the NAC(+) group had a significantly lower score in the Ex cluster than the NAC(−) group (Figure 3G, above). Furthermore, the immune suppression signature scores (Table S3) in Treg of the tumor tissue were compared between NAC(−) and NAC(+) groups, and the NAC(+) group showed a significantly lower score in the Treg cluster than the NAC(−) group (Figure 3G). We also performed the same analyses using the data only from surgical samples and found the similar significant differences in the signature scores between the NAC(+) and NAC(−) groups (Figure S5).

In this comparison of the NAC(+) group with the NAC(−) group, we found that there was Th1 with higher memory ability, Ex of CD4T with a lower exhaust score, and Treg with lower cytotoxicity and lower immune suppressive ability in the NAC(+) group than in the NAC(−) group, suggesting that NAC promotes the anti-tumor immune response in each CD4T cluster.

NAC enhanced the anti-tumor immune response of each DC cluster in the TME

To analyze antigen-presenting myeloid cells, we extracted *ITGAM*+ and/or *ITGAX*+ cells from *HLA-DRA*+ cells of Figure 1B (Figures S6A, S6B). A total of 15,338 cells were extracted, and 4,673 cells were excluded as doublet or contamination cells (Figure S6C). The remaining cells were divided into five clusters (Figure S6D) on the basis of DEGs (Figure S6E, Table S2) and representative gene expression (Figure S6F). Next, 740 DCs were extracted and re-clustered (Figure 4A) on the basis of gene expression characteristics (Figures 4B and 4C, Figure S7, and Table S2). Previous studies reported that cDC1 presents antigen mainly to CD8T[19] and cDC2 mainly to CD4T.[20] However, both *HLA-A*, coding a component of major histocompatibility complex (MHC) class I, and *HLA-DRA*, coding a component of MHC class II, were highly expressed in cDC1 (Figure 4B), which is consistent with recent reports that cDC1 acquires the ability to induce anti-tumor immunity to CD8T by priming CD4T.[21]

There was no remarkable difference in the proportion of DC clusters between normal mucosa and tumor tissue or between NAC(+) and NAC(−) groups in tumor tissue (Figure 4D). The NAC(+) group showed a significantly higher score of the antigen presentation-related active signature in the cDC1 cluster and a significantly lower score in the DC_CCR7 cluster than the NAC(−) group (Figure 4E). The score of the dysfunction signature, which is involved in suppression of the anti-tumor immune response in other immune cells, was significantly lower in the cDC2 and DC_CCR7 clusters of the NAC(+) group than that in the NAC(−) group (Figure 4E). In addition, the migration signature scores in the cDC1 and cDC2 clusters of the NAC(+) group were significantly higher than that of the NAC(−) group, while not significantly different in the DC_CCR7 cluster (Figure 4E). We also performed the same analyses using the data only from surgical samples and found the similar significant differences in the signature scores except for the

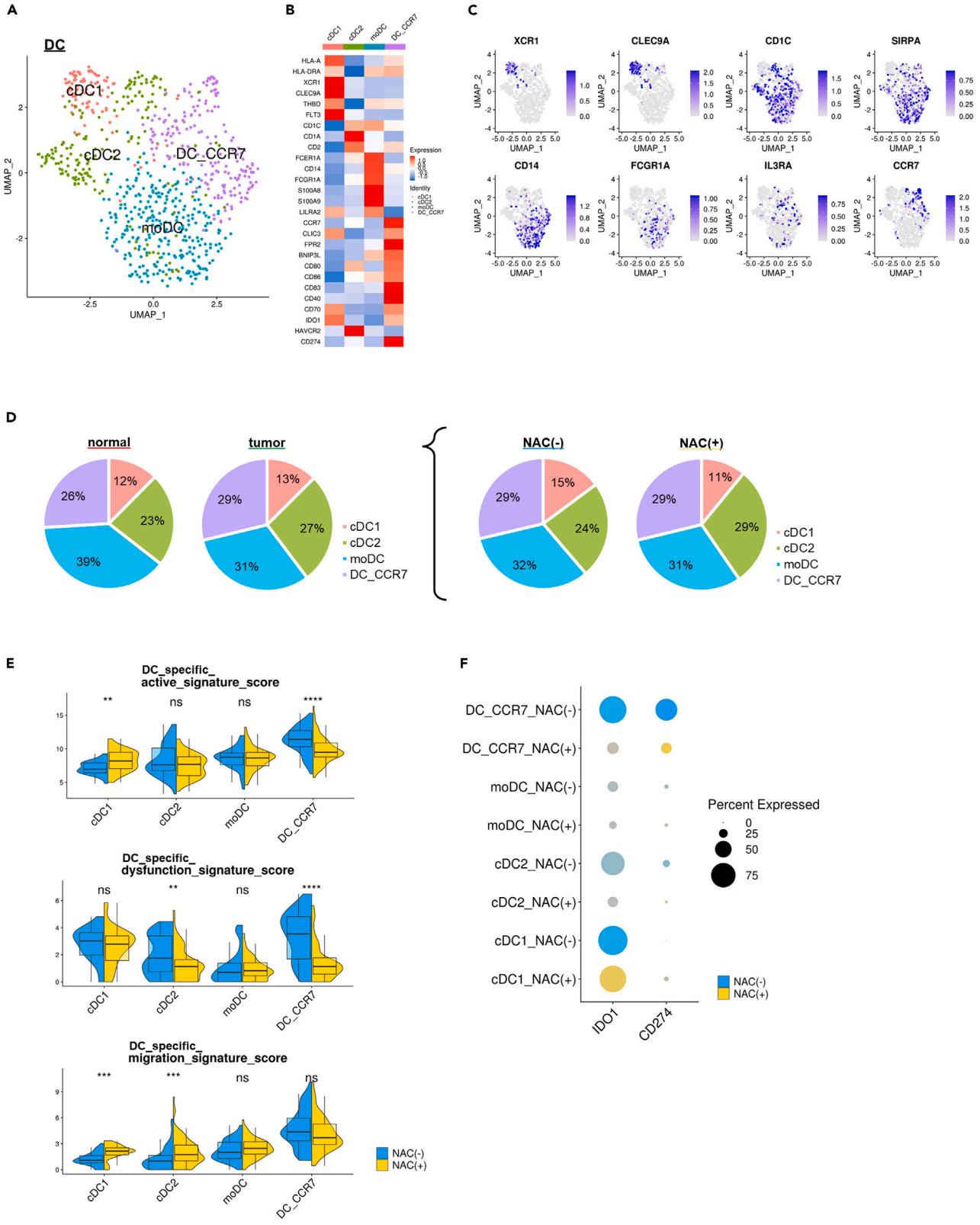
A
DC
cDC1
cDC2
DC_CCR7
moDC
UMAP_1
UMAP_2
B
cDC1
cDC2
moDC
DC_CCR7
HLA-A
HLA-DRA
XCR1
CLEC9A
THBD
FLT3
CD1C
CD1A
CD2
FCER1A
CD14
FCGR1A
S100A8
S100A9
LILRA2
CCR7
CLIC3
FPR2
BNIP3L
CD80
CD86
CD83
CD40
CD70
IDO1
HAVCR2
CD274
Expression
Identity
C
XCR1
CLEC9A
CD1C
SIRPA
CD14
FCGR1A
IL3RA
CCR7
UMAP_1
UMAP_2
D
normal
tumor
NAC(-)
NAC(+)
12%
23%
39%
26%
13%
27%
31%
29%
15%
24%
32%
29%
11%
29%
31%
29%
cDC1
cDC2
moDC
DC_CCR7
E
DC_specific_
active_signature_score
DC_specific_
dysfunction_signature_score
DC_specific_
migration_signature_score
**
ns
ns
****
***
cDC1
cDC2
moDC
DC_CCR7
NAC(-)
NAC(+)
F
DC_CCR7_NAC(-)
DC_CCR7_NAC(+)
moDC_NAC(-)
moDC_NAC(+)
cDC2_NAC(-)
cDC2_NAC(+)
cDC1_NAC(-)
cDC1_NAC(+)
IDO1
CD274
Percent Expressed
0
25
50
75
NAC(-)
NAC(+)

Figure 4. NAC enhanced the anti-tumor immune response of each DC cluster in the TME

(A) UMAP plot of 740 DCs extracted from myeloid cells. The cell types of each cluster were determined based on the gene expression.

(B) Heatmap of representative gene expression.

(C) Expression of representative marker genes in UMAP.

(D) Percentage of the number of cells composing each cluster. The top graphs show normal mucosa and tumor tissue, and the bottom graphs are shown by the presence of NAC in the tumor tissue.

(E) Comparison of signature gene expression in tumor tissue with and without NAC. The violin plots were drawn based on the scored signature gene expression in each cell.

(F) Comparison of *IDO1* and *CD274* gene expression in tumor tissue with and without NAC. The size of the dots indicates the percentage of expressing cells in the cluster, and the brightness of the dots indicates the expression level of the cluster. **DC**, dendritic cell; **MKI67**, MKI67 rich cell; **HSP**, heat shock protein cell; **cDC1**, conventional DC type1; **cDC2**, conventional DC type2; **moDC**, monocyte-derived DC; **DC_CCR7**, CCR7 rich DC; **normal**, normal mucosa; **tumor**, tumor tissue; **NAC**, neoadjuvant chemotherapy; **ns**, not significant; *, $p < 0.05$; **, $p < 0.01$; ***, $p < 0.001$; ****, $p < 0.0001$.

See also Figures S6, S7, S8, Tables S2, and S3.

active signature of cDC2 (Figure S8). *IDO1* and *CD274* included in the gene set of dysfunction signature were expressed at lower levels in cDC2 and DC_CCR7 in the NAC(+) group than in the NAC(−) group (Figure 4F).

These results suggest that NAC enhances the anti-tumor immune response on each DC cluster via enhancement of the antigen presentation function in cDC1 and the migration of cDC1 and cDC2 and decrease of the immune suppressive activity of cDC2 and DC_CCR.

NAC enhances anti-tumor activity in each cluster of Mφ via the increased chemotaxis and the decreased suppressive function

From the cells of Figure 4A, the Mφ cluster was extracted and divided into four clusters (Figure 5A). The expressions of *CD80* and *CD86*, which are representative genes of M1 macrophages with anti-tumor abilities,[22] and *CD163* and *MRC1*, which are representative genes of M2 macrophages with tumor-promoting activities,[23] were all predominant in cluster 4 and their distribution did not characterize the four clusters identified in Figure 5A (Figure 5B). In the trajectory analysis, we observed the transition from cluster 1 through cluster 2 to cluster 3 and cluster 4 (Figure 5C). We investigated highly expressed genes in each cluster (Figure 5D, Figure S9, and Table S2) and found that each cluster showed a gene expression pattern related with the specific function as shown in Figure 5D. The percentage of the M_phagocytosis cluster was remarkably low, and the percentage of the M_mature cluster was remarkably high in tumor tissue compared with the percentages in the normal mucosa (Figure 5E). In the tumor tissue, there was no remarkable difference in the proportion of each cluster between NAC(+) and NAC(−) groups (Figure 5E). However, when we calculated the signature score based on expression of the specific function-related genes in each cluster (Table S3), we found that the chemotaxis score of the M_cytokine and M_mature clusters was significantly higher in the NAC(+) group than in the NAC(−) group. Furthermore, in the M_mature cluster, the anti-tumor active score of Mφ was high in both groups, whereas the score of the suppressive signature involved in the inhibition of the anti-tumor active function of Mφ in tumor immunity was significantly lower in the NAC(+) group than in the NAC(−) group. (Figure 5F). We also performed the same analyses using the data only from surgical samples and found that the active signature score of the M_mature cluster was also high in both groups although the score was significantly lower in the NAC(+) group than in the NAC(−) group (Figure S10).

These data suggest that NAC increased the chemotaxis of the M_cytokine and M_mature clusters and decreased the anti-tumor suppressive function of the M_mature cluster, possibly leading to the enhanced anti-tumor activity of Mφ.

NAC promotes the interactions among immune cell clusters in the TME to enhance their anti-tumor immune responses

In the present study, we identified the clusters based on single cell gene expression in CD8T, CD4T, antigen-presenting myeloid cells, DCs, and Mφ. To understand how these clusters interact with each other, we performed "NicheNetR" analysis, which is a package for evaluating intercellular communication. In this analysis, the priority of ligands on the sending cells are estimated according to the changes in gene expression observed in the receiving cells, and the expressed genes on the receiving cells that are regulated by the inferred ligands are searched for as target genes.[24]

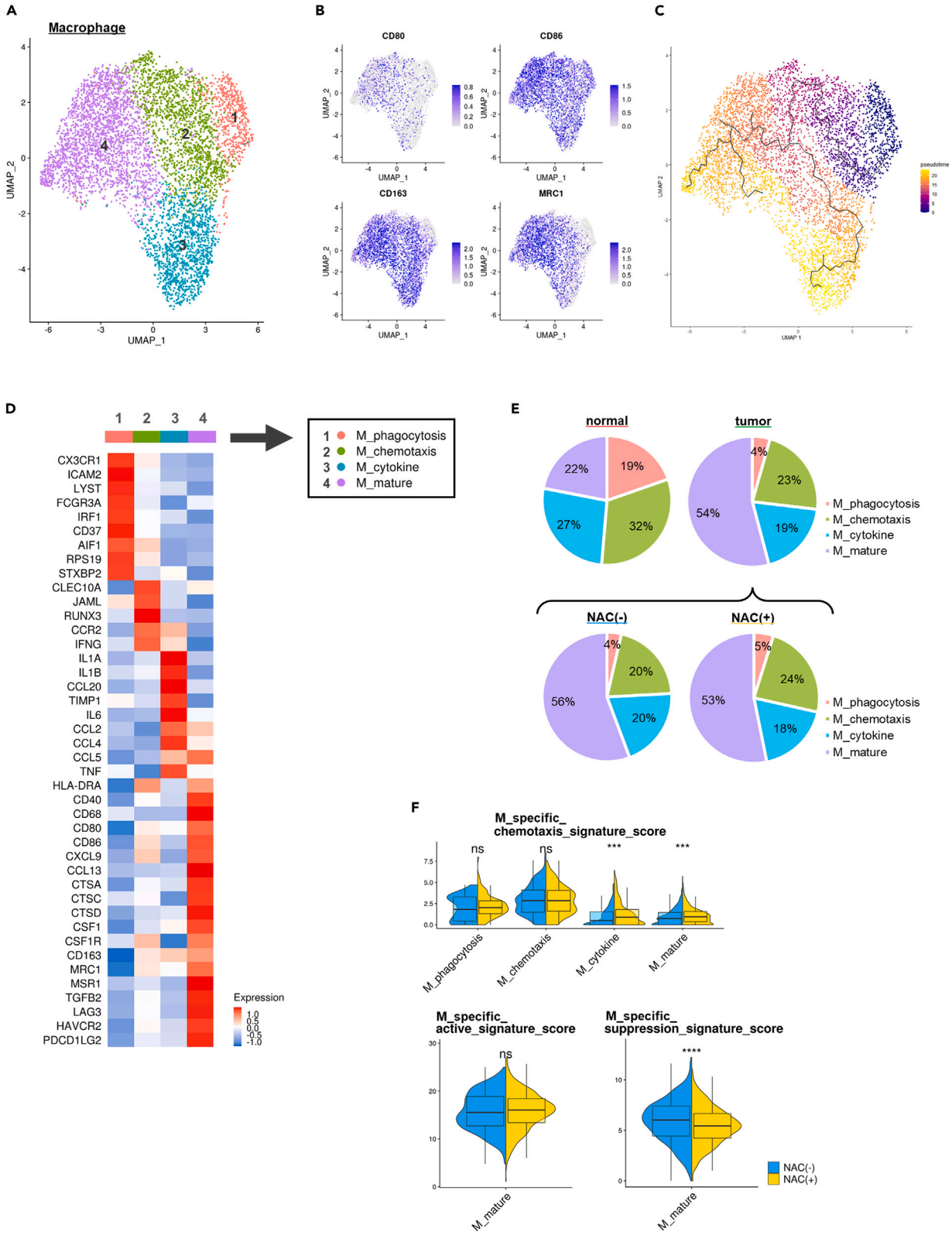
A
Macrophage
UMAP_1
UMAP_2
1
2
3
4
B
CD80
CD86
CD163
MRC1
C
pseudotime
D
1 2 3 4
CX3CR1
ICAM2
LYST
FCGR3A
IRF1
CD37
AIF1
RPS19
STXBP2
CLEC10A
JAML
RUNX3
CCR2
IFNG
IL1A
IL1B
CCL20
TIMP1
IL6
CCL2
CCL4
CCL5
TNF
HLA-DRA
CD40
CD68
CD80
CD86
CXCL9
CCL13
CTSA
CTSC
CTSD
CSF1
CSF1R
CD163
MRC1
MSR1
TGFB2
LAG3
HAVCR2
PDCD1LG2
Expression
1 M_phagocytosis
2 M_chemotaxis
3 M_cytokine
4 M_mature
E
normal
tumor
22%
19%
27%
32%
4%
23%
54%
19%
M_phagocytosis
M_chemotaxis
M_cytokine
M_mature
NAC(-)
NAC(+)
4%
20%
56%
20%
5%
24%
53%
18%
F
M_specific_
chemotaxis_signature_score
ns
ns
***
***
M_phagocytosis
M_chemotaxis
M_cytokine
M_mature
M_specific_
active_signature_score
ns
M_mature
M_specific_
suppression_signature_score
****
M_mature
NAC(-)
NAC(+)

Figure 5. NAC enhances anti-tumor activity in each cluster of Mφ via the increased chemotaxis and the decreased suppressive function

(A) UMAP plot of 5,756 macrophages extracted from myeloid cells. The cells were divided into four clusters.

(B) Expression of representative marker genes for M1 and M2 in UMAP.

(C) Trajectory analysis of macrophages. The pseudotime trajectory was calculated with darker colors indicating older and lighter colors indicating newer.

(D) Heatmap of representative gene expression. From this gene expression pattern, the function of each cluster was determined as shown in the figure.

(E) Percentage of the number of cells composing each cluster. The top graphs show normal mucosa and tumor tissue, and the bottom graphs are shown as the presence of NAC in the tumor tissue.

(F) Comparison of signature gene expression in tumor tissue with and without NAC. The violin plots were drawn on the basis of the scored signature gene expression in each cell. **M**, macrophage; **normal**, normal mucosa; **tumor**, tumor tissue; **NAC**, neoadjuvant chemotherapy; **ns**, not significant; *, $p < 0.05$; **, $p < 0.01$; ***, $p < 0.001$; ****, $p < 0.0001$.

See also Figures S9, S10, Tables S2, and S3.

We set Treg cluster as targets to analyze cluster interactions, and several differences in the gene expression of Treg between the NAC(+) and NAC(−) groups and genes of other clusters that affect the expression of Treg genes were identified (Figure 6A). We focused on the expression of *FOXP3* and *IL2RB*. In this study, Eff cluster of CD8T, Th1 cluster, and Ex cluster of CD4T were the main *IFNG*-producing clusters. CD8T Eff and CD4T Th1 clusters showed a significantly high level of *IFNG* expression in the NAC(+) group compared with that in the NAC(−) group (Figure 6F). *IFNG* was previously reported to suppress *FOXP3* expression in Treg and contributes to the anti-tumor effect.[25] We also found that the expression of *EBI3*, which confers a suppression activity of Treg,[26] was significantly decreased in the DC_CCR7 cluster of the NAC group (Figure 6F). These data also suggest that NAC altered the function of CD8T Eff, CD4T Th1, and DC_CCR7 clusters, possibly leading to suppression of Treg function in the TME.

IDO1 in DC has been shown to activate Treg and suppress non-Treg T cells, leading to immune escape of tumors.[27,28] *IDO1* expression was significantly lower in the cDC2 and DC_CCR7 clusters of the NAC(+) group than in the NAC(−) group. In addition, *IL4I1* expression, which interferes with T cell proliferation,[29] was also significantly reduced in the DC_CCR7 cluster of the NAC(+) group (Figures 6B and 6C). Among the main *IFNG*-producing clusters, only the Ex cluster of CD4T had significantly lower *IFNG* expression in the NAC(+) group than in NAC(−) group (Figure 6F). Considering that previous reports showed that *IDO1* in DCs is induced by *IFNG*,[30] these data suggest the possibility that the Ex cluster of CD4T plays a role in reducing *IDO1* expression in DCs and enhancing the anti-tumor effect during NAC.

Among the genes selected in the analysis of the M_chemotaxis cluster, the expressions of *CD36*, *NEAT1*, *PRDM1*, and *PTGS2*, all of which are upregulated through the NF-κB pathway and exert tumor-promoting function when expressed in Mφ,[31–34] were significantly lower in the NAC(+) group than in the NAC(−) group (Figure 6D). Significantly low expression of *NAMPT* in various clusters of Mφ in the NAC(+) group was observed (Figure 6F). *NAMPT* has been shown to increase NF-κB pathway activity.[35] These data suggest that low *NAMPT* expression in Mφ of the NAC(+) group contributes to the anti-tumor environment via downregulation of these genes in the M_chemotaxis cluster.

The expression of *IL10* was also significantly lower in the M_mature cluster of the NAC(+) group than in the NAC(−) group (Figure 6E). *IL10* derived from tumor-infiltrating Mφ promotes cancer stem cell-like properties of cancer cells through the JAK/STAT pathway.[36] In addition, *IL10* production in Mφ is suppressed by *IFNG*.[37] As mentioned in the Treg section, the CD8T Eff and CD4T Th1 clusters of the NAC(+) group had a significantly higher level of *IFNG* expression than the NAC(−) group among the main *IFNG*-producing clusters (Figure 6F). These findings suggest that the *IFNG* produced by CD8T Eff and CD4T Th1 clusters suppressed the *IL10*-mediated tumor-promoting ability of the M_mature cluster.

DISCUSSION

In the present study, we used scRNA-seq to analyze the NAC-induced changes in the immunological TME of human ESCC. Data on $CD45^+$ cells were analyzed, focusing on CD8T, CD4T, DCs, and Mφ. The results showed that CD8T and CD4T were functionally repartitioned into six clusters each, and DCs and Mφ were functionally repartitioned into four clusters each. We then compared function-related gene expression in the immune cell clusters of the NAC(+) group with that of the NAC(−) group and found the following results. In the NAC(+) group, almost all CD8T clusters avoid apoptosis and exhaustion, the Th1 cluster is more memorized and avoids exhaustion. Both Treg cytotoxic and suppression ability are lower, and the antigen presentation in the cDC1 cluster is higher. Dysfunction signatures were lower in both cDC2 and DC_CCR7 clusters, migration was enhanced in cDC1/2 clusters, chemotaxis was higher in M_cytokine

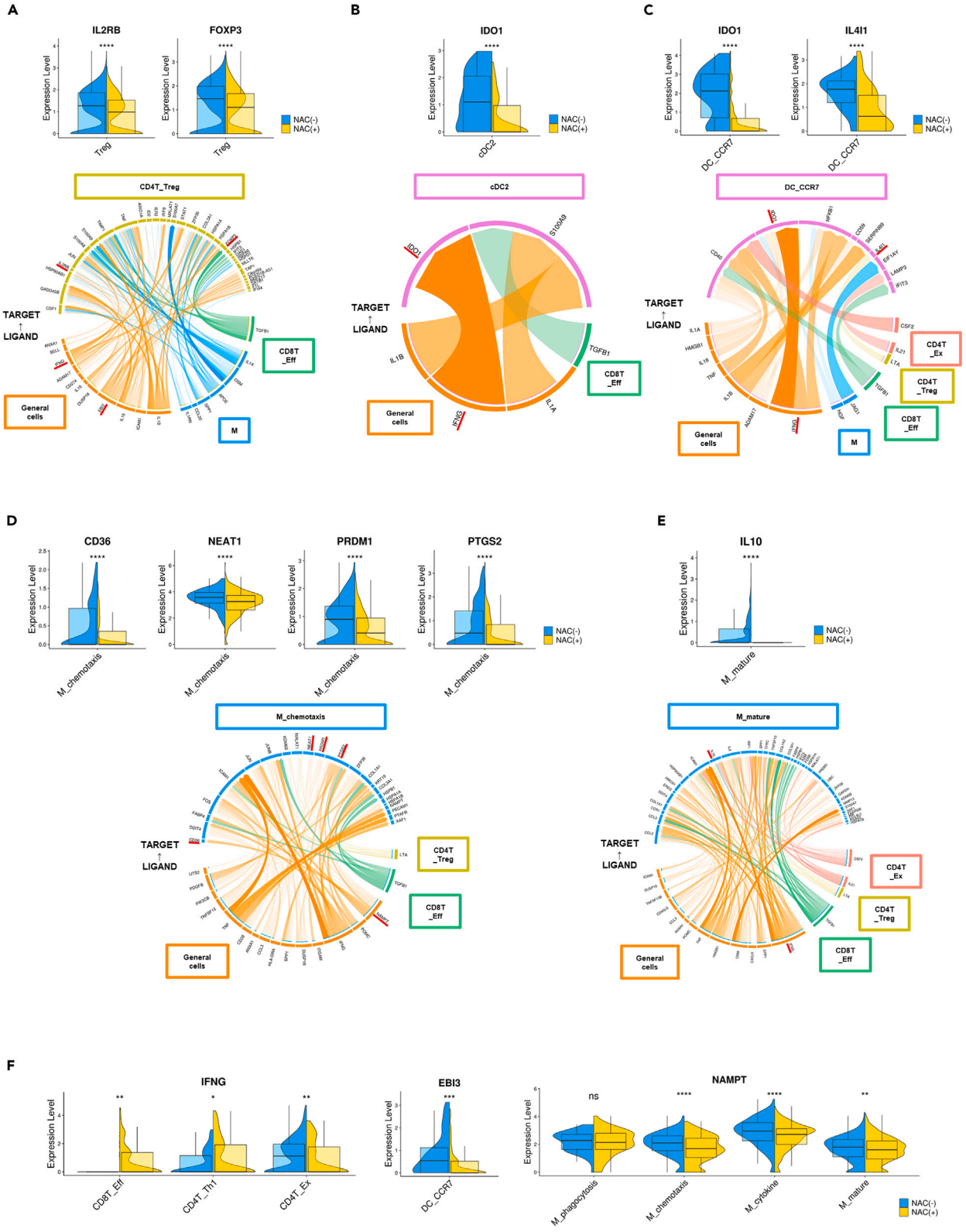
A
IL2RB
FOXP3
Expression Level
Treg
NAC(-)
NAC(+)
CD4T_Treg
TARGET
LIGAND
CD8T _Eff
General cells
M
B
IDO1
cDC2
cDC2
S100A9
IDO1
IL1B
TGFB1
IL1A
IFNG
CD8T _Eff
General cells
C
IDO1
IL4I1
DC_CCR7
DC_CCR7
CD4T _Ex
CD4T _Treg
CD8T _Eff
M
General cells
D
CD36
NEAT1
PRDM1
PTGS2
M_chemotaxis
M_chemotaxis
CD4T _Treg
CD8T _Eff
General cells
E
IL10
M_mature
M_mature
CD4T _Ex
CD4T _Treg
CD8T _Eff
General cells
F
IFNG
CD8T_Eff
CD4T_Th1
CD4T_Ex
EBI3
DC_CCR7
NAMPT
ns
M_phagocytosis
M_chemotaxis
M_cytokine
M_mature

Figure 6. NAC promotes the interactions among immune cell clusters in the TME to enhance their anti-tumor immune responses

(A–E) Interactions between clusters evaluated up to Figure 5. The lower half of the circle shows the ligand genes labeled as "LIGAND." The ligand genes identified in multiple clusters are shown as "General cells." The upper half of the circle shows the genes that were eventually produced by the receptors that responded to the identified ligands; these genes are labeled as "TARGET." The receiver clusters for analysis were specified as (A) Treg, (B) cDC2, (C) DC_CCR7, (D) M_chemotaxis, and (E) M_mature. Each violin plot compares gene expression in the cells that can influence tumor progression in the receiver cluster of tumor tissue with and without NAC.

(F) Cluster-wise comparison of the expression of genes identified as "LIGAND" that could influence the "TARGET.". **CD8T**, $CD8^+$ T cell; **Eff**, effector CD8T; **CD4T**, $CD4^+$ T cell; **N**, naive CD4T; **Tfh**, follicular helper CD4T; **Th1**, type 1 helper CD4T; **Treg**, regulatory CD4T; **Ex**, exhausted cell; **DC**, dendritic cell; **cDC2**, conventional DC type2; **DC_CCR7**, CCR7 rich DC; **M**, macrophage; **normal**, normal mucosa; **tumor**, tumor tissue; **NAC**, neoadjuvant chemotherapy; **ns**, not significant; *, $p < 0.05$; **, $p < 0.01$; ***, $p < 0.001$; ****, $p < 0.0001$.

and M_mature clusters, and the suppression function was decreased in the M_mature cluster while anti-tumor activity was maintained. These data suggest that the functions of all immune cells within the TME were altered to an enhanced anti-tumor immune response, although the effects of NAC differed among the functional clusters even within each specific cell type. We further focused on the interactions among immune cell clusters and found the following: the NAC(+) group showed significantly higher expression of *IFNG* in CD4T Th1 and CD8T Eff clusters and reduced immune suppressive activity in the Treg cluster with decreased *FOXP3* and *IL2RB* expression, whereas a significant decrease in *IFNG* expression in the CD4T Ex cluster was linked to a decrease in *IDO1* and *IL4I1* expression in the cDC2 and DC_CCR7 clusters during NAC. The decrease in *EBI3* expression in the DC_CCR7 cluster was also linked to the decrease in *FOXP3* and *IL2RB* expression in Treg during NAC. The increase in *IFNG* expression in CD4T Th1 and CD8T Eff clusters was linked to the decrease in *IL10* expression in Mφ. The decrease in *NAMPT* expression in Mφ was linked to the decrease in *CD36*, *NEAT1*, *PRDM1*, and *PTGS2* expression in the M_chemotaxis cluster. Taken together, these data suggest that NAC affected functional clusters individually and their interactions with each other enhanced the anti-tumor immune response in the ESCC TME during NAC.

The "cancer-immune cycle" in the anti-tumor immune response is a cycle divided into seven steps that has been widely recognized.[38] Disruption of this cycle is thought to lead to cancer growth, invasion, metastasis, and resistance to treatment. Chemotherapy has been reported to affect various cells involved in this cycle. Di Caro et al.[39] reported that TGFβ reprogrammed tumor-associated macrophages into an inflammatory phenotype. In human colorectal cancer, cyclophosphamide reduced the number of peripheral B cells and Treg,[40] and irinotecan reduced peripheral Treg.[41] Furthermore, cisplatin increased the cytotoxicity of NK cells in human hepatocellular carcinoma.[42] However, these reports only evaluated the responses of a certain immune cell type, and there have been no studies to date that have comprehensively analyzed NAC-induced changes in the single cell-based gene expression of various immune cell types in the TME of human ESCC. In this study, we subdivided known immune cell types to functional clusters based on single cell gene expression and comprehensively evaluated the effects of NAC on the function of each cluster. These results indicated that NAC-induced specific interactions among immune cell clusters across cell types, leading to enhancement of the anti-tumor immune response of human ESCC.

In the present analysis of CD8T, the Eff cluster showed extremely strong expression of cytotoxic genes such as *GZMB* and *PRF1* and almost no expression of exhaust genes such as *PDCD1* and *LAG3*, suggesting that the Eff cluster is a cytotoxic cluster in CD8T. However, a recent report demonstrated that CD8T exposed to antigens immediately begin to express exhaust genes.[43] Therefore, there is a possibility that the Eff cluster observed in this study is a cluster of bystander CD8T that have not been exposed to specific tumor antigens and do not possess tumor-killing abilities.[44] On the other hand, the EM and Ex clusters of CD8T in this study had high expression of both cytotoxic and exhaust gene expression, suggesting that such clusters could recognize specific tumor antigens during their activation.

In this study, the DC_CCR7 cluster had a high migration signature, and the antigen presentation ability of the DC_CCR7 cluster was higher than that of the other DC clusters in both NAC(+) and NAC(−) groups. These data suggest that the DC_CCR7 cluster could include DCs, which take up antigen and migrate to lymph nodes to present antigen during the cancer-immune cycle.[38] Furthermore, in the analysis of the DC_CCR7 cluster, the expression level of genes related with the suppressive functions for the anti-tumor immune response of other immune cells was lower in the NAC(+) group than in the NAC(−) group, although the antigen presentation ability was lower in the DC_CCR7 cluster of the NAC(+) group than the NAC(−) group. These present data suggest that NAC promoted the migration of DCs, especially

DCs in the DC_CCR7 cluster with high antigen presentation ability and suppressive function, to lymph nodes, possibly contributing to acceleration of the cancer-immune cycle.

Conventionally, tumor-infiltrating Mφ is classified as anti-tumor M1 and tumor-promoting M2.[22] However, in the present analyses of Mφ, we found that the known M1 and M2 marker gene[22,23] expression broadly overlapped in most cell clusters of Mφ. Compared with the other clusters, the M_mature cluster showed higher expression of antigen presentation-related genes such as genes encoding co-stimulation factors and *HLA-DRA*, coding a component of MHC class II, as well as cathepsin-related genes that have an anti-tumor effect on macrophages.[45] M2-related genes and immune checkpoint genes including *LAG3* and *HAVCR2* (known as *TIM-3*) were also highly expressed in the M_mature cluster. These data suggest that the conventional M1 and M2 were included in the M_mature cluster, and the conventional classification of Mφ in the TME into M1 and M2 may not be appropriate for understanding the functional heterogeneity of Mφ. To further understand the function and the differentiation process of Mφ clusters, we performed trajectory analysis using the expression of characteristic genes and the results categorized Mφ into four clusters. These four clusters had distinctly different functions based on gene expression, suggesting that this clustering is a promising classification for understanding the functional heterogeneity of Mφ in the TME.

In the present study, we investigated the effects of NAC on the immunological TME of ESCC using scRNA-seq. The results suggest that NAC enhanced the anti-tumor immune response of functional clusters of various immune cell types in the TME. In addition, the multiple immune cell clusters with functions altered by NAC interacted with each other, resulting in an enhanced anti-tumor immune response. Such a comprehensive understanding of the NAC-induced changes in functional clusters of various immune cell types will contribute to the establishment of optimal combination treatments targeting the TME during NAC.

Limitations of the study

This study has several limitations. First, several kinds of NAC regimens were included in this study, and the dosage varied depending on the general condition of the patient. Furthermore, since the indication for NAC was determined according to the preoperative diagnosis, the staging of the disease was not standardized according to the with or without NAC. In addition, characteristics of tumor after NAC were also individualized. Moreover, the NAC(−) group includes biopsy samples and surgical specimens, whereas the NAC(+) group included only surgical specimens. Therefore, a comparative analyses with a larger number of samples that are collected in the same method and *in vivo*/vitro experiments with homogeneous conditions are required to assess the effect of NAC on the immunological TME of ESCC.

STAR★METHODS

Detailed methods are provided in the online version of this paper and include the following:

- KEY RESOURCES TABLE
- RESOURCE AVAILABILITY
  - Lead contact
  - Materials availability
  - Data and code availability
- EXPERIMENTAL MODEL AND SUBJECT DETAILS
  - Sample collection
- METHOD DETAILS
  - Sample preparation
  - scRNA-seq library preparation and sequencing
  - scRNA-seq data analysis
- QUANTIFICATION AND STATISTICAL ANALYSIS

SUPPLEMENTAL INFORMATION

Supplemental information can be found online at https://doi.org/10.1016/j.isci.2023.106480.

ACKNOWLEDGMENTS

The authors would like to thank E. Manabe and S. Sadatomi (Department of Surgery and Oncology, Kyushu University Hospital, Fukuoka, Japan) for their technical assistance during experiments. The computation

was carried out using the computer resource offered under the category of general projects by Research Institute for Information Technology, Kyushu University. This work was supported by JSPS KAKENHI Grant Numbers JP19H03732, JP20K17621, JP20K17622, JP21K08800, JP21K19530, and JP21K19531. We thank Gabrielle White Wolf, PhD, from Edanz (https://www.edanz.com/) for editing a draft of this manuscript.

AUTHOR CONTRIBUTIONS

S.O.: Conceptualization, data curation, formal analysis, investigation, methodology, project administration, software, visualization, and writing – original draft.

K.O.: Conceptualization, formal analysis, funding acquisition, methodology, project administration, resources, supervision, and writing – review & editing.

S.N.: Data curation, formal analysis, investigation, methodology, software, validation, and visualization.

C.T.: Data curation, formal analysis, investigation, methodology, software, validation, and visualization.

K.H.: Data curation, formal analysis, investigation, methodology, software, validation, and visualization.

Y.M.: Methodology and validation.

J.K.: Resources.

Y.O.: Data curation, formal analysis, investigation, methodology, software, validation, and visualization.

T.S.: Investigation and validation.

C.I.: Investigation, methodology, and validation.

N.T.: Formal analysis, funding acquisition, and software.

Y.M.: Funding acquisition and project administration.

K.S.: Project administration and resources.

T.M.: Funding acquisition, project administration, resources, and supervision.

K.N.: Project administration and supervision.

T.T.: Resources, supervision, and writing – review & editing.

T.M.: Supervision and writing – review & editing.

T.K.: Resources, supervision, and writing – review & editing.

Y.O.: Resources, supervision, and writing – review & editing.

M.N.: Conceptualization, funding acquisition, supervision, and writing – review & editing.

DECLARATION OF INTERESTS

The authors declare no competing interests.

INCLUSION AND DIVERSITY

We support inclusive, diverse, and equitable conduct of research.

Received: September 11, 2022
Revised: February 8, 2023
Accepted: March 19, 2023
Published: March 21, 2023

REFERENCES

1. Bray, F., Ferlay, J., Soerjomataram, I., Siegel, R.L., Torre, L.A., and Jemal, A. (2018). Global cancer statistics 2018: GLOBOCAN estimates of incidence and mortality worldwide for 36 cancers in 185 countries. CA. Cancer J. Clin. *68*, 394–424. https://doi.org/10.3322/caac.21492.

2. Watanabe, M., Tachimori, Y., Oyama, T., Toh, Y., Matsubara, H., Ueno, M., Kono, K., Uno, T., Ishihara, R., Muro, K., et al. (2021). Comprehensive registry of esophageal cancer in Japan, 2014. Esophagus *18*, 1–24. https://doi.org/10.1007/s10388-020-00785-y.

3. Kamarajah, S.K., Navidi, M., Wahed, S., Immanuel, A., Hayes, N., Griffin, S.M., and Phillips, A.W. (2020). Significance of neoadjuvant downstaging in carcinoma of esophagus and gastroesophageal junction. Ann. Surg Oncol. *27*, 3182–3192. https://doi.org/10.1245/s10434-020-08358-0.

4. Hiraki, Y., Kimura, Y., Imano, M., Kato, H., Iwama, M., Shiraishi, O., Yasuda, A., Shinkai, M., Makino, T., Motoori, M., et al. (2021). Controlling lymph node micrometastases by neoadjuvant chemotherapy affects the prognosis in advanced esophageal squamous cell carcinoma. Surg. Today *51*, 118–126. https://doi.org/10.1007/s00595-020-02059-7.

5. Ando, N., Kato, H., Igaki, H., Shinoda, M., Ozawa, S., Shimizu, H., Nakamura, T., Yabusaki, H., Aoyama, N., Kurita, A., et al. (2012). A randomized trial comparing postoperative adjuvant chemotherapy with cisplatin and 5-fluorouracil versus preoperative chemotherapy for localized advanced squamous cell carcinoma of the thoracic esophagus (JCOG9907). Ann. Surg Oncol. *19*, 68–74. https://doi.org/10.1245/s10434-011-2049-9.

6. Ohigashi, Y., Sho, M., Yamada, Y., Tsurui, Y., Hamada, K., Ikeda, N., Mizuno, T., Yoriki, R., Kashizuka, H., Yane, K., et al. (2005). Clinical significance of programmed death-1 ligand-1 and programmed death-1 ligand-2 expression in human esophageal cancer. Clin. Cancer Res. *11*, 2947–2953. https://doi.org/10.1158/1078-0432.CCR-04-1469.

7. Kato, K., Cho, B.C., Takahashi, M., Okada, M., Lin, C.Y., Chin, K., Kadowaki, S., Ahn, M.J., Hamamoto, Y., Doki, Y., et al. (2019). Nivolumab versus chemotherapy in patients with advanced oesophageal squamous cell carcinoma refractory or intolerant to previous chemotherapy (ATTRACTION-3): a multicentre, randomised, open-label, phase 3 trial. Lancet Oncol. *20*, 1506–1517. https://doi.org/10.1016/S1470-2045(19)30626-6.

8. Fukuoka, E., Yamashita, K., Tanaka, T., Sawada, R., Sugita, Y., Arimoto, A., Fujita, M., Takiguchi, G., Matsuda, T., Oshikiri, T., et al. (2019). Neoadjuvant chemotherapy increases PD-L1 expression and CD8+ tumor-infiltrating lymphocytes in esophageal squamous cell carcinoma. Anticancer Res. *39*, 4539–4548. https://doi.org/10.21873/ANTICANRES.13631.

9. Liang, Y., Yu, M., Zhou, C., and Zhu, X. (2020). Variation of PD-L1 expression in locally advanced cervical cancer following neoadjuvant chemotherapy. Diagn. Pathol. *15*, 67–68. https://doi.org/10.1186/s13000-020-00977-1.

10. Li, H., van der Leun, A.M., Yofe, I., Lubling, Y., Gelbard-Solodkin, D., van Akkooi, A.C.J., van den Braber, M., Rozeman, E.A., Haanen, John B.A.G., Blank, C.U., et al. (2019). Dysfunctional CD8 T cells form a proliferative, dynamically regulated compartment within human melanoma. Cell *176*, 775–789.e18. https://doi.org/10.1016/j.cell.2018.11.043.

11. Guo, X., Zhang, Y., Zheng, L., Zheng, C., Song, J., Zhang, Q., Kang, B., Liu, Z., Jin, L., Xing, R., et al. (2018). Global characterization of T cells in non-small-cell lung cancer by single-cell sequencing. Nat. Med. *24*, 978–985. https://doi.org/10.1038/S41591-018-0045-3.

12. Penter, L., Dietze, K., Ritter, J., Lammoglia Cobo, M.F., Garmshausen, J., Aigner, F., Bullinger, L., Hackstein, H., Wienzek-Lischka, S., Blankenstein, T., et al. (2019). Localization-associated immune phenotypes of clonally expanded tumor-infiltrating T cells and distribution of their target antigens in rectal cancer. OncoImmunology *8*, e1586409. https://doi.org/10.1080/2162402X.2019.1586409.

13. Savas, P., Virassamy, B., Ye, C., Salim, A., Mintoff, C.P., Caramia, F., Salgado, R., Byrne, D.J., Teo, Z.L., Dushyanthen, S., et al. (2018). Single-cell profiling of breast cancer T cells reveals a tissue-resident memory subset associated with improved prognosis. Nat. Med. *24*, 986–993. https://doi.org/10.1038/s41591-018-0078-7.

14. Zheng, Y., Chen, Z., Han, Y., Han, L., Zou, X., Zhou, B., Hu, R., Hao, J., Bai, S., Xiao, H., et al. (2020). Immune suppressive landscape in the human esophageal squamous cell carcinoma microenvironment. Nat. Commun. *11*, 6268. https://doi.org/10.1038/s41467-020-20019-0.

15. Huang, R., Zhu, L., and Zhang, Y. (2020). XIST lost induces ovarian cancer stem cells to acquire taxol resistance via a KMT2C-dependent way. Cancer Cell Int. *20*, 436. https://doi.org/10.1186/s12935-020-01500-8.

16. Anderson, A.M., Kalimutho, M., Harten, S., Nanayakkara, D.M., Khanna, K.K., and Ragan, M.A. (2017). The metastasis suppressor RARRES3 as an endogenous inhibitor of the immunoproteasome expression in breast cancer cells. Sci. Rep. *7*, 39873. https://doi.org/10.1038/srep39873.

17. Blum, W., Pecze, L., Rodriguez, J.W., Steinauer, M., and Schwaller, B. (2018). Regulation of calretinin in malignant mesothelioma is mediated by septin 7 binding to the CALB2 promoter. BMC Cancer *18*, 475. https://doi.org/10.1186/s12885-018-4385-7.

18. He, Z., Thorrez, L., Siegfried, G., Meulemans, S., Evrard, S., Tejpar, S., Khatib, A.M., and Creemers, J.W.M. (2020). The proprotein convertase furin is a pro-oncogenic driver in KRAS and BRAF driven colorectal cancer. Oncogene *39*, 3571–3587. https://doi.org/10.1038/s41388-020-1238-z.

19. Cancel, J.C., Crozat, K., Dalod, M., and Mattiuz, R. (2019). Are conventional type 1 dendritic cells critical for protective antitumor immunity and how? Front. Immunol. *10*, 9. https://doi.org/10.3389/fimmu.2019.00009.

20. Binnewies, M., Mujal, A.M., Pollack, J.L., Combes, A.J., Hardison, E.A., Barry, K.C., Tsui, J., Ruhland, M.K., Kersten, K., Abushawish, M.A., et al. (2019). Unleashing type-2 dendritic cells to drive protective antitumor CD4+ T cell immunity. Cell *177*, 556–571.e16. https://doi.org/10.1016/J.CELL.2019.02.005.

21. Ferris, S.T., Durai, V., Wu, R., Theisen, D.J., Ward, J.P., Bern, M.D., Davidson, J.T., Bagadia, P., Liu, T., Briseño, C.G., et al. (2020). cDC1 prime and are licensed by CD4+ T cells to induce anti-tumour immunity. Nature *584*, 624–629. https://doi.org/10.1038/s41586-020-2611-3.

22. Wu, K., Lin, K., Li, X., Yuan, X., Xu, P., Ni, P., and Xu, D. (2020). Redefining tumor-associated macrophage subpopulations and functions in the tumor microenvironment. Front. Immunol. *11*, 1731. https://doi.org/10.3389/fimmu.2020.01731.

23. Jayasingam, S.D., Citartan, M., Thang, T.H., Mat Zin, A.A., Ang, K.C., and Ch'ng, E.S. (2019). Evaluating the polarization of tumor-associated macrophages into M1 and M2 phenotypes in human cancer tissue: technicalities and challenges in routine clinical practice. Front. Oncol. *9*, 1512. https://doi.org/10.3389/fonc.2019.01512.

24. Browaeys, R., Saelens, W., and Saeys, Y. (2020). NicheNet: modeling intercellular communication by linking ligands to target genes. Nat. Methods *17*, 159–162. https://doi.org/10.1038/s41592-019-0667-5.

25. Overacre-Delgoffe, A.E., Chikina, M., Dadey, R.E., Yano, H., Brunazzi, E.A., Shayan, G., Horne, W., Moskovitz, J.M., Kolls, J.K., Sander, C., et al. (2017). Interferon-γ drives Treg fragility to promote anti-tumor

immunity. Cell *169*, 1130–1141.e11. https://doi.org/10.1016/j.cell.2017.05.005.

26. Park, Y.J., Ryu, H., Choi, G., Kim, B.S., Hwang, E.S., Kim, H.S., and Chung, Y. (2019). IL-27 confers a protumorigenic activity of regulatory T cells via CD39. Proc. Natl. Acad. Sci. USA *116*, 3106–3111. https://doi.org/10.1073/pnas.1810254116.

27. Holmgaard, R.B., Zamarin, D., Munn, D.H., Wolchok, J.D., and Allison, J.P. (2013). Indoleamine 2,3-dioxygenase is a critical resistance mechanism in antitumor T cell immunotherapy targeting CTLA-4. J. Exp. Med. *210*, 1389–1402. https://doi.org/10.1084/jem.20130066.

28. Fu, C., and Jiang, A. (2018). Dendritic cells and CD8 T cell immunity in tumor microenvironment. Front. Immunol. *9*, 3059. https://doi.org/10.3389/fimmu.2018.03059.

29. Boulland, M.L., Marquet, J., Molinier-Frenkel, V., Möller, P., Guiter, C., Lasoudris, F., Copie-Bergman, C., Baia, M., Gaulard, P., Leroy, K., and Castellano, F. (2007). Human IL4I1 is a secreted L-phenylalanine oxidase expressed by mature dendritic cells that inhibits T-lymphocyte proliferation. Blood *110*, 220–227. https://doi.org/10.1182/blood-2006-07-036210.

30. Hwu, P., Du, M.X., Lapointe, R., Do, M., Taylor, M.W., and Young, H.A. (2000). Indoleamine 2,3-dioxygenase production by human dendritic cells results in the inhibition of T cell proliferation. J. Immunol. *164*, 3596–3599. https://doi.org/10.4049/jimmunol.164.7.3596.

31. Su, P., Wang, Q., Bi, E., Ma, X., Liu, L., Yang, M., Qian, J., and Yi, Q. (2020). Enhanced lipid accumulation and metabolism are required for the differentiation and activation of tumor-associated macrophages. Cancer Res. *80*, 1438–1450. https://doi.org/10.1158/0008-5472.CAN-19-2994.

32. Gao, Y., Fang, P., Li, W.J., Zhang, J., Wang, G.P., Jiang, D.F., and Chen, F.P. (2020). LncRNA NEAT1 sponges miR-214 to regulate M2 macrophage polarization by regulation of B7-H3 in multiple myeloma. Mol. Immunol. *117*, 20–28. https://doi.org/10.1016/j.molimm.2019.10.026.

33. Severa, M., Islam, S.A., Waggoner, S.N., Jiang, Z., Kim, N.D., Ryan, G., Kurt-Jones, E., Charo, I., Caffrey, D.R., Boyartchuk, V.L., et al. (2014). The transcriptional repressor BLIMP1 curbs host defenses by suppressing expression of the chemokine CCL8. J. Immunol. *192*, 2291–2304. https://doi.org/10.4049/jimmunol.1301799.

34. Prima, V., Kaliberova, L.N., Kaliberov, S., Curiel, D.T., and Kusmartsev, S. (2017). COX2/mPGES1/PGE2 pathway regulates PD-L1 expression in tumor-associated macrophages and myeloid-derived suppressor cells. Proc. Natl. Acad. Sci. USA *114*, 1117–1122. https://doi.org/10.1073/pnas.1612920114.

35. Lin, Y.C., Wu, H.C., Liao, C.C., Chou, Y.C., Pan, S.F., and Chiu, C.M. (2015). Secretion of one adipokine Nampt/visfatin suppresses the inflammatory stress-induced NF- B activity and affects Nampt-dependent cell viability in huh-7 cells. Mediators Inflamm. *2015*, 392471. https://doi.org/10.1155/2015/392471.

36. Yang, L., Dong, Y., Li, Y., Wang, D., Liu, S., Wang, D., Gao, Q., Ji, S., Chen, X., Lei, Q., et al. (2019). IL-10 derived from M2 macrophage promotes cancer stemness via JAK1/STAT1/NF-κB/Notch1 pathway in non-small cell lung cancer. Int. J. Cancer *145*, 1099–1110. https://doi.org/10.1002/ijc.32151.

37. Hu, X., Paik, P.K., Chen, J., Yarilina, A., Kockeritz, L., Lu, T.T., Woodgett, J.R., and Ivashkiv, L.B. (2006). IFN-Γ suppresses IL-10 production and synergizes with TLR2 by regulating GSK3 and CREB/AP-1 proteins. Immunity *24*, 563–574. https://doi.org/10.1016/j.immuni.2006.02.014.

38. Chen, D.S., and Mellman, I. (2013). Oncology meets immunology: the cancer-immunity cycle. Immunity *39*, 1–10. https://doi.org/10.1016/j.immuni.2013.07.012.

39. di Caro, G., Cortese, N., Castino, G.F., Grizzi, F., Gavazzi, F., Ridolfi, C., Capretti, G., Mineri, R., Todoric, J., Zerbi, A., et al. (2016). Dual prognostic significance of tumour-Associated macrophages in human pancreatic adenocarcinoma treated or untreated with chemotherapy. Gut *65*, 1710–1720. https://doi.org/10.1136/gutjnl-2015-309193.

40. Scurr, M., Pembroke, T., Bloom, A., Roberts, D., Thomson, A., Smart, K., Bridgeman, H., Adams, R., Brewster, A., Jones, R., et al. (2017). Low-dose cyclophosphamide induces antitumor T-cell responses, which associate with survival in metastatic colorectal cancer. Clin. Cancer Res. *23*, 6771–6780. https://doi.org/10.1158/1078-0432.CCR-17-0895.

41. Roselli, M., Formica, V., Cereda, V., Jochems, C., Richards, J., Grenga, I., Orlandi, A., Ferroni, P., Guadagni, F., and Schlom, J. (2016). The association of clinical outcome and peripheral T-cell subsets in metastatic colorectal cancer patients receiving first-line FOLFIRI plus bevacizumab therapy. OncoImmunology *5*, e1188243. https://doi.org/10.1080/2162402X.2016.1188243.

42. Shi, L., Lin, H., Li, G., Sun, Y., Shen, J., Xu, J., Lin, C., Yeh, S., Cai, X., and Chang, C. (2016). Cisplatin enhances NK cells immunotherapy efficacy to suppress HCC progression via altering the androgen receptor (AR)-ULBP2 signals. Cancer Lett. *373*, 45–56. https://doi.org/10.1016/j.canlet.2016.01.017.

43. Ahn, E., Araki, K., Hashimoto, M., Li, W., Riley, J.L., Cheung, J., Sharpe, A.H., Freeman, G.J., Irving, B.A., and Ahmed, R. (2018). Role of PD-1 during effector CD8 T cell differentiation. Proc. Natl. Acad. Sci. USA *115*, 4749–4754. https://doi.org/10.1073/pnas.1718217115.

44. Simoni, Y., Becht, E., Fehlings, M., Loh, C.Y., Koo, S.L., Teng, K.W.W., Yeong, J.P.S., Nahar, R., Zhang, T., Kared, H., et al. (2018). Bystander CD8+ T cells are abundant and phenotypically distinct in human tumour infiltrates. Nature *557*, 575–579. https://doi.org/10.1038/s41586-018-0130-2.

45. Shree, T., Olson, O.C., Elie, B.T., Kester, J.C., Garfall, A.L., Simpson, K., Bell-Mcguinn, K.M., Zabor, E.C., Brogi, E., and Joyce, J.A. (2011). Macrophages and cathepsin proteases blunt chemotherapeutic response in breast cancer. Genes Dev. *25*, 2465–2479. https://doi.org/10.1101/gad.180331.111.

46. Stuart, T., Butler, A., Hoffman, P., Hafemeister, C., Papalexi, E., Mauck, W.M., Hao, Y., Stoeckius, M., Smibert, P., and Satija, R. (2019). Comprehensive integration of single-cell data. Cell *177*, 1888–1902.e21. https://doi.org/10.1016/j.cell.2019.05.031.

47. Cao, J., Spielmann, M., Qiu, X., Huang, X., Ibrahim, D.M., Hill, A.J., Zhang, F., Mundlos, S., Christiansen, L., Steemers, F.J., et al. (2019). The single-cell transcriptional landscape of mammalian organogenesis. Nature *566*, 496–502. https://doi.org/10.1038/s41586-019-0969-x.

48. Nestorowa, S., Hamey, F.K., Pijuan Sala, B., Diamanti, E., Shepherd, M., Laurenti, E., Wilson, N.K., Kent, D.G., and Göttgens, B. (2016). A single-cell resolution map of mouse hematopoietic stem and progenitor cell differentiation. Blood *128*, e20–e31. https://doi.org/10.1182/blood-2016-05-716480.

49. Hafemeister, C., and Satija, R. (2019). Normalization and variance stabilization of single-cell RNA-seq data using regularized negative binomial regression. Genome Biol. *20*, 296. https://doi.org/10.1101/576827.

STAR★METHODS

KEY RESOURCES TABLE

REAGENT or RESOURCE	SOURCE	IDENTIFIER
Chemicals, peptides, and recombinant proteins		
Liberase™ TH Research Grade	Merck	Cat# 5401135001
Bovine serum albumin	Merck	Cat# A9418
TrypLE Express (1X), phenol red	Thermo Fisher Scientific	Cat# 12605010
Red Blood Cell Lysis Solution (10X)	Miltenyi Biotec	Cat# 130-094-183
Dead Cell Removal Kit	Miltenyi Biotec	Cat# 130-090-101
Buffer EB	QIAGEN	Cat# 19086
10% Tween 20	Bio-Rad	Cat#1610781
Critical commercial assays		
Chromium Next GEM Single Cell 3' Reagent Kit v3.1	10x Genomics	Cat# 1000121
Chromium Next GEM Chip G Single Cell Kit	10x Genomics	Cat# 1000120
Single Index Kit T Set A	10x Genomics	Cat# 1000213
SPRIselect beads	Beckman Coulter	Cat# B23318
Agilent High Sensitivity DNA Kit	Agilent	Cat# 5067-4626
Deposited data		
Single cell RNA sequencing for esophageal squamous cell carcinoma	This paper	[Database]: [GSE197677]
Experimental models: Organisms/strains		
Human / esophageal squamous cell carcinoma or normal mucosa	This paper	Table S1
Software and algorithms		
R v3.6.3	R Foundation for Statistical Computing	https://www.r-project.org/
Seurat v3.1.5	Stuart, et al., 2019[46]	https://satijalab.org/seurat/
Monocle3	Cao, et al., 2019[47]	https://cole-trapnell-lab.github.io/monocle3/
NicheNetR	Browaeys, et al., 2020[24]	https://github.com/saeyslab/nichenetr

RESOURCE AVAILABILITY

Lead contact

Further information and requests for resources and reagents should be directed to and will be fulfilled by the lead contact, Kenoki Ohuchida (ouchida.kenoki.060@m.kyushu-u.ac.jp).

Materials availability

This study did not generate new unique reagents.

Data and code availability

- Single-cell RNA-seq data have been deposited at GEO and are publicly available as of the date of publication. Accession numbers are listed in the key resources table.
- This paper does not report original code.
- Any additional information required to reanalyze the data reported in this paper is available from the lead contact upon request.

EXPERIMENTAL MODEL AND SUBJECT DETAILS

Sample collection

Nineteen patients who were pathologically diagnosed with ESCC were enrolled in this study, irrespective of sex. The clinical information of patients is summarized in Table S1. Specimens of 14 patients were obtained from excised tissue at the time of surgery, and specimens of 5 patients were obtained as biopsies during gastroscopy. Among the surgical specimens, 13 ESCC tissue and 12 normal mucosa were collected; 9 of the 13 ESCC tissue and 7 of the 12 normal mucosa samples were from patients treated with NAC. Five biopsy samples were all ESCC tissue and from patients not treated with chemotherapy.

All samples were collected at the Department of Surgery and Oncology, Kyushu University Hospital (Fukuoka, Japan) between October 2019 and February 2021. Tumor staging was classified according to AJCC/UICC TNM Classification of Malignant Tumors, 8th Edition (46). All studies were performed in accordance with the Declaration of Helsinki and were approved by the institutional review board of the Kyushu University Hospital (2022-100). Written informed consent was obtained from all patients.

METHOD DETAILS

Sample preparation

Samples were immediately rinsed with PBS, minced into <1 mm^3 pieces on ice, transferred to 10 mL digestion buffer containing Liberase™ TH (1 mg, Merck, Darmstadt Germany) and TryPLE Express (1 mL, Thermo Fisher, Waltham, Massachusetts, USA), and incubated for 20 min in a 37°C water bath with continuous manual shaking. Samples were then mixed with pipetting for 1 min, added 30 mL of ice-cold PBS containing 2% fetal bovine serum, and passed through a 70 μm cell strainer (Corning, NY, USA). Following centrifugation (300 g, 4°C, 5 min), the pellet was resuspended in Red Blood Cell Lysis Solution 10X (0.2 mL, Miltenyi Biotec, Bergisch Gladbach, Germany) incubated at room temperature for 5 min, and centrifuged (300 g, 4°C, 5 min). The pellet was resuspended in 1 mL PBS containing 0.1% bovine serum albumin (Merck). Finally, the cells were treated using a Dead Cell Removal Kit (Miltenyi Biotec) and passed through a 40 μm cell strainer (Corning). The obtained single cell suspension was used for scRNA-seq.

scRNA-seq library preparation and sequencing

Libraries for scRNA-seq were generated using the Chromium Next GEM Single Cell 3' Reagent Kit v3.1 (10x Genomics, Pleasanton, California, USA). We aimed to profile 10,000 cells per library. All libraries were sequenced on the NovaSeq6000 (Illumina, San Diego, California, USA) or DNBSEQ-G400 (MGI Tech, Shenzhen, China) and the sequence reads number was set at 50,000 reads per cell.

scRNA-seq data analysis

Raw sequencing reads were aligned to the human reference genome GRCh38 and processed to a matrix representing the UMI's per cell barcode per gene using Cell Ranger v5.0.0 (10x Genomics). The output files were analyzed with the R v3.6.3 package "Seurat v3.1.5".[46] Low-quality cells (<100 UMI/cell, >6,000 UMI/cell, and >50% mitochondrial genes) were excluded and only $CD45^+$ cells were extracted. We used the "CellCycleScoring"[48] function for all samples to mitigate the effects of cell cycle heterogeneity in scRNA-seq data by calculating cell cycle phase scores based on canonical markers and regressing these out of the data during pre-processing. To merge the data of all samples, we used the "SCTransform"[49] package for the normalization and variance stabilization of molecular count data. After principal component analysis using the "RunPCA" function, clusters were calculated by the "FindNeighbors" and "FindClusters" function and visualized using the dimensional reduction method "UMAP". The trajectories of the cells in the clusters were analyzed by "Monocle3"[47] and intercellular communication was evaluated using "NicheNetR".[24]

QUANTIFICATION AND STATISTICAL ANALYSIS

To evaluate the gene expression, we used the "VlnPlot" function and the "geom_boxplot" function. The "Vlnplot" was used to draw the distribution of gene expression for each cell. In the boxplot, each box represented the median and interquartile range (IQR, 25th–75th percentile range) of the data, and whiskers indicated the largest and lowest values within 1.5 times the IQR. Statistical analysis was performed using "stat_compare_means" function to compare two groups by Wilcoxon test. The threshold for significance was $p<0.05$.